Supporting information

Small−Strain Niobium Nitride Anode with Ordered Mesopores for Ultra−Stable Potassium−Ion Batteries

Jisung Lee,[a,†] Seongseop Kim,[a,†] Jae−Hyuk Park,[b,c,†] Changshin Jo,[d] Jinyoung Chun,[e] Yung−Eun Sung,[b,c,*] Eunho Lim,[f,*] and Jinwoo Lee[a,*]

[a] Department of Chemical and Biomolecular Engineering, Korea Advanced Institute of Science and Technology (KAIST), Daejeon 34141, Republic of Korea

[b] Center for Nanoparticle Research, Institute for Basic Science (IBS), Seoul 08826, Republic of Republic of Korea

[c] School of Chemical and Biological Engineering, Seoul National University (SNU), Seoul 08826, Republic of Korea

[d] Department of Engineering, University of Cambridge, Cambridge CB3 0FS, UK,

[e] Energy & Environment Division, Korea Institute of Ceramic Engineering & Technology (KICET), Jinju 52851, Republic of Korea

[f] Carbon Resources Institute, Korea Research Institute of Chemical Technology (KRICT), Daejeon 34114, Republic of Korea

Methods

Materials. Poly(ethylene oxdie)−*block*−poly(styrene) (PEO−*b*−PS) and phenol−formaldehyde resin (resol) were synthesized by using reported methods. Monomethoxy PEO (mPEO, 5000 g mol^{-1}), phenol, formaldehyde solution (36.5−38% in H_2O), and niobium ethoxide ($Nb(OEt)_5$) were purchased from Sigma−Aldrich. Sodium hydroxide (NaOH, bead), tetrahydrofuran (THF) (HPLC grade), and concentrated HCl (35−37%) were purchased from Samchun (Korea).

Synthesis of PEO−*b*−PS. PEO−*b*−PS was prepared by atom transfer radical polymerization (ATRP). It consists of two steps, preparation of mPEO−Br macroinitiator and polymerization of styrene to form PEO−*b*−PS. 20 g of monomethoxy PEO (mPEO, 5000 g mol^{-1}) was dissolved in 200 ml of CH_2Cl_2 and 6 ml of excess TEA was added. The solution was placed in an ice−bath, and 1.48 ml of 2−bromoisobutylbromide was injected slowly under stirring. After reaction at room temperature for 24 h, the resulting solution was purified by extraction in water and precipitation in ether. After filtration to collect PEO−Br, it was dry under vacuum at 40 °C. To polymerize styrene for PEO−*b*−PS, 2.539 g of PEO−Br, 20 g of styrene, 0.071 g of CuBr and 0.085 PMDETA were placed in a 50 ml round bottom flask. The mixture was degassed by freeze−pump−thaw and immersed in an oil bath at 90 °C for overnight. The polymerized product was cooled down to room temperature and was dissolved in THF. The solution was filtered through neutral alumina column to remove the catalyst. The filtered solution was added in the cold methanol to precipitate PEO−*b*−PS, followed by drying under vacuum at 40 °C.

Synthesis of phenol−formaldehyde resin (resol). 5 g of phenol was melted and mixed slowly with 1.1 g of 20 wt% of NaOH aqueous solution under stirring. After 10 min, 8.6 g of formaldehyde solution was added to basic phenol solution. The solution reacted at 70 °C for 1 h with stirring and

cooled down at room temperature, sequentially. 2M HCl was added to the solution to neutralize and water was removed in a vacuum oven at 45 °C. THF was poured into the flask with resol. NaCl generated during neutralization was precipitated and resol was dissolved in THF. After the removal of NaCl by filtration, THF was removed under vacuum condition at 45 °C.

Material Characterization. Gel permeation chromatography (GPC; Waters) was performed using THF as the eluent, and the molar mass was calibrated on the basis of PS standards. The nanostructure was investigated by transmission electron microscopy (TEM, JEM−1011, Jeol LTD) operated at 80 kV and scanning electron microscopy (SEM, S−4200 field emission SEM, Hitach) operated at 30 kV. The nitrogen physisorption was carried out at 77 K using a Tristar II 3020 (Micromeritics Instrument Co.). All samples were degassed at 110 °C for 24 hours before measurements. Pore size was estimated from the adsorption branch of N2 gas isotherm by Barret−Joyner−Halenda (BJH) method. Specific surface area was determined by Brunauer–Emmett–Teller (BET) method. Powder X−ray diffraction (XRD) patterns were obtained using Rigaku D/MAX−2500/PC X−ray diffractometer using Cu−Kα radiation (λ = 0.154 nm). Small-angle X−ray scattering (SAXS) measurements were carried out on the 4C SAXS beamline at the Pohang Light Source II.

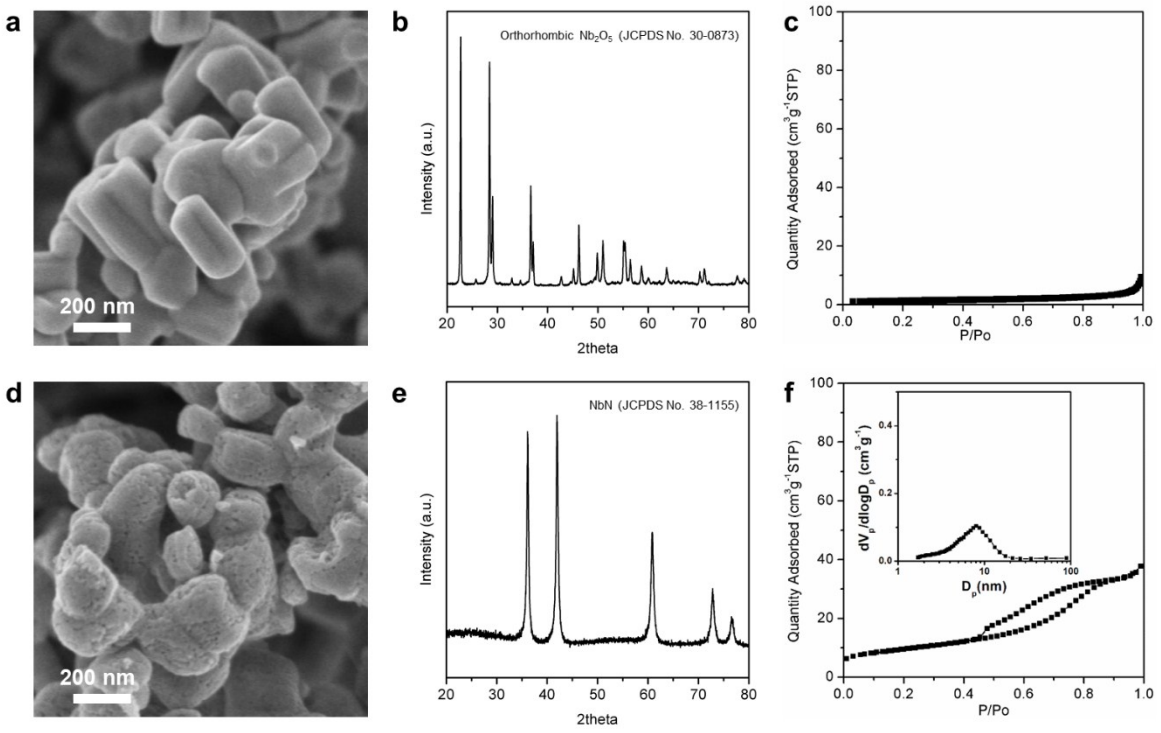

Fig. S1. Characterization of commercial Nb_2O_5 (c−Nb_2O_5) and NbN (c−NbN). (a) SEM image, (b) XRD pattern consistent with orthorhombic phase, and (c) N_2 physisorption isotherm of c−Nb_2O_5. (d) SEM image, (e) XRD pattern consistent with cubic phase, (f) N_2 physisorption isotherm, and corresponding pore size distribution (inset) of c−NbN.

SEM image shows that c−Nb_2O_5 possesses nonporous structures and irregular particle shapes (Fig. S1a). XRD pattern of c−Nb_2O_5 corresponds to highly crystalline orthorhombic phase and the average crystallite size is about 46.5 nm (Fig. S1b). The BET surface area of c−Nb_2O_5 is 5 m^2 g^{-1} (Fig. S1c). To prepare c−NbN, we converted c−Nb_2O_5 into c−NbN by heat treatment at 700 °C under NH_3 for 5 h. During the nitridation, c−Nb_2O_5 severely shrinks as a result of phase transition from orthorhombic to cubic, leading to porous structures (Fig. S1d). The crystallite size of c−NbN

decreases to 18.8 nm due to the phase shrinkage (Fig. S1e). c−NbN possesses the surface area of 33 $m^2 g^{-1}$ and the pore size of 8 nm (Fig. S1f).

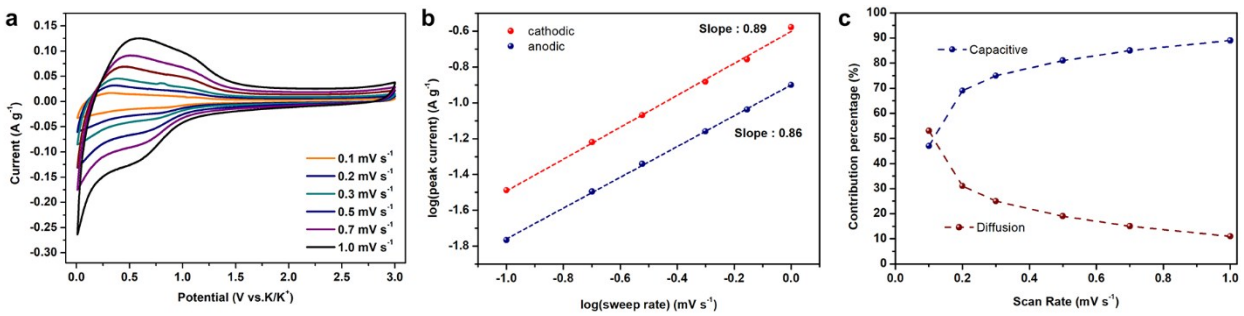

Fig. S2. Kinetic analysis of c−NbN (a) CV curves and (b) specific peak currents of c−NbN at various scan rates. (c) Capacitive contribution percentage of c−NbN.

The kinetics of K^+ storage was investigated with CV curves as the same method described in the main manuscript. Fig. S2 shows CV curves at different scan rates, indicating the shape of CV curves is maintained well. The *b*−values of cathodic and anodic at specific peak currents are 0.89 and 0.86, respectively, confirming electrode of c−NbN shows pseudo−capacitive characteristic. Fig. S2c exhibits the percentage of contribution of capacitive and diffusion-controlled reaction. The proportions of capacitive contributions are 53 and 70% at scan rates of 0.1 and 0.2 mV s^{-1}, respectively, demonstrating pseudo−capacitive charge storage is one of the intrinsic properties of niobium nitride.

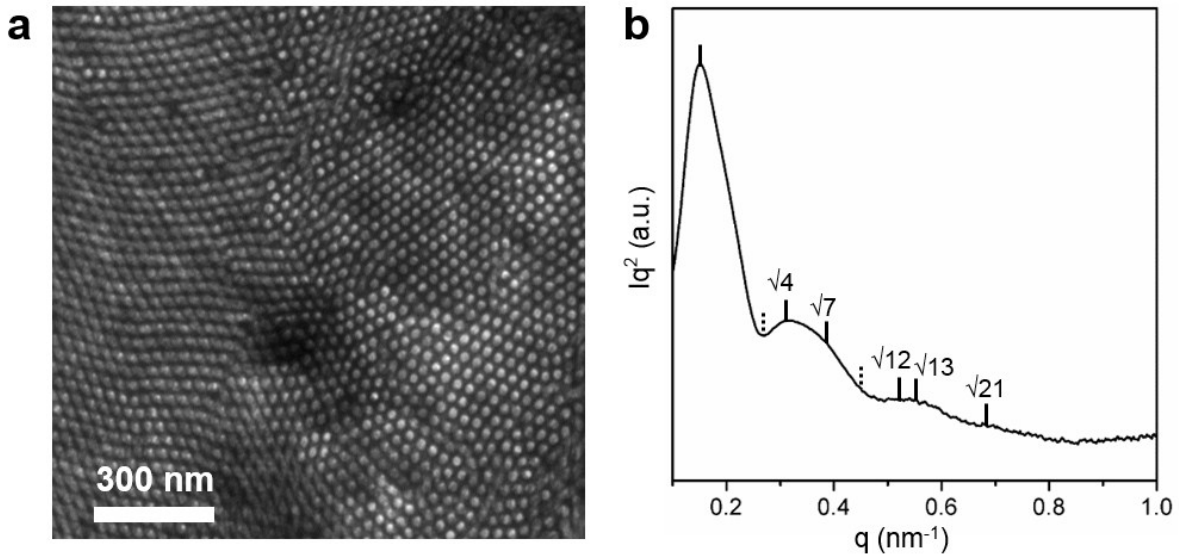

Fig. S3. Characterization of as−made BCP/NbO_x/resol hybrid. (a) TEM image and (b) SAXS pattern consistent with 2D hexagonal structure (*p6mm*).

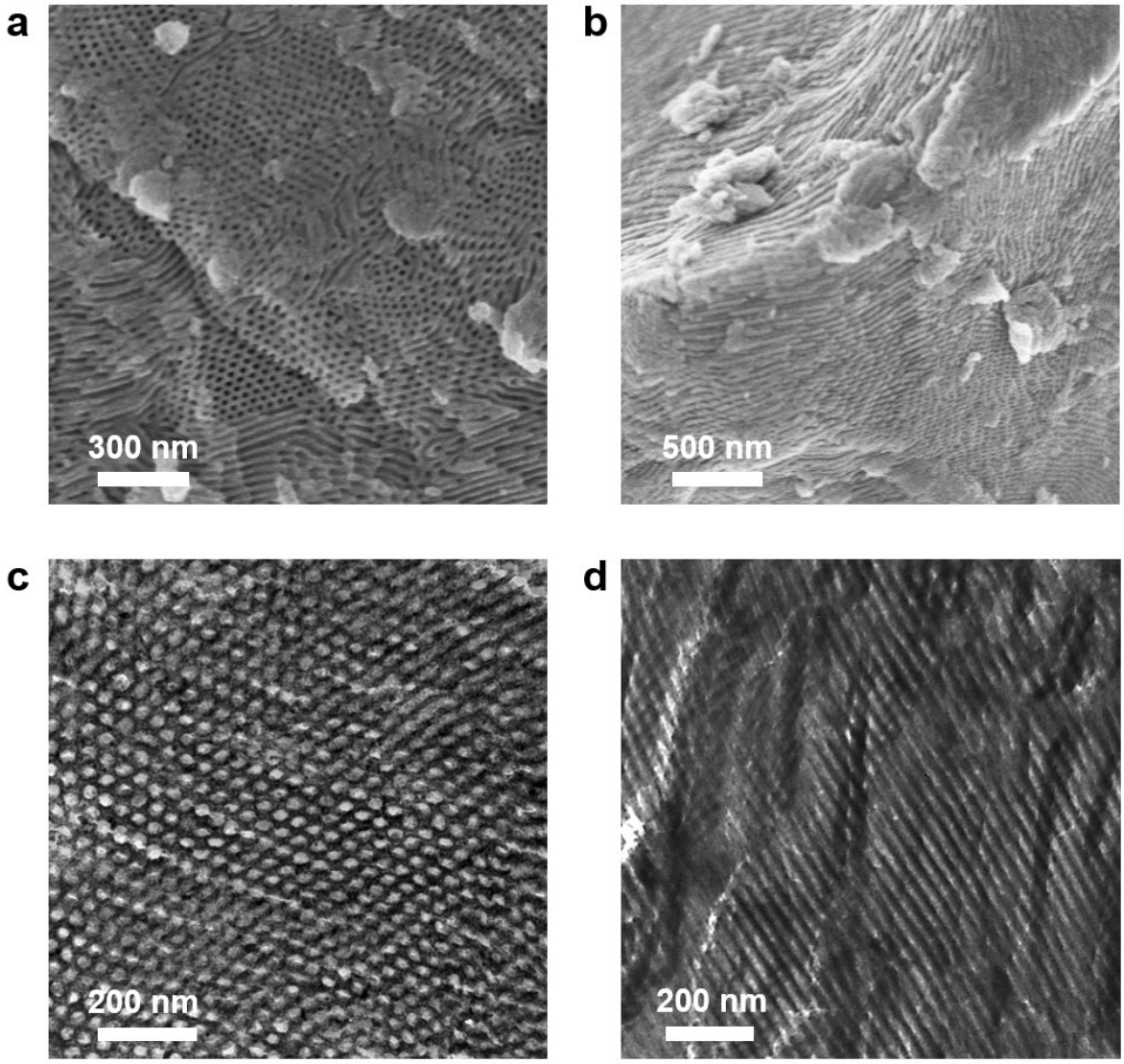

Fig. S4. (a, b) SEM and (c, d) TEM images of m−Nb_2O_5/C.

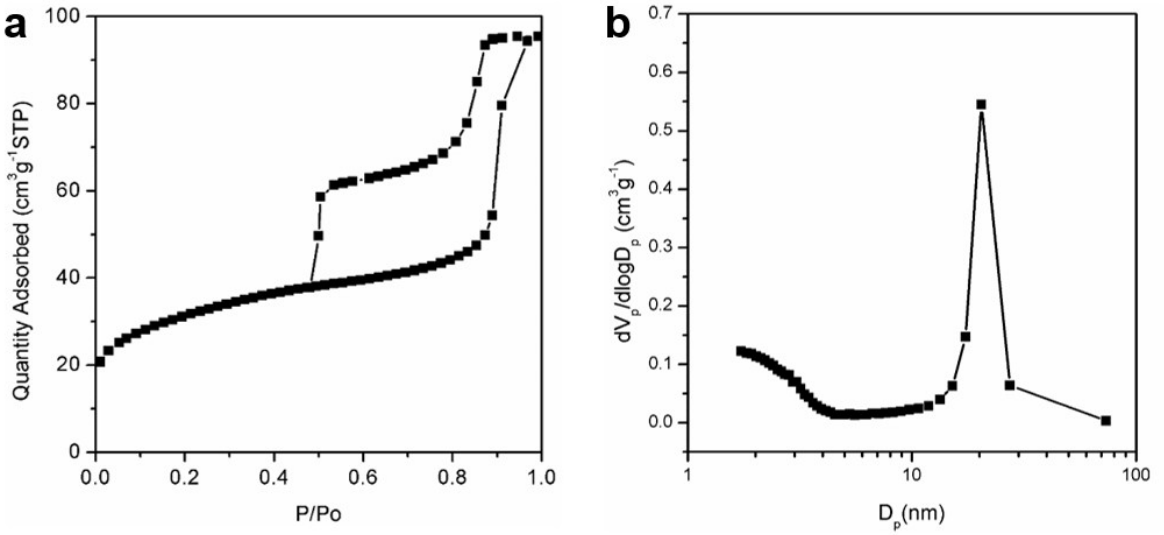

Fig. S5. (a) N_2 physisorption isotherm and (b) corresponding pore size distribution of the m−Nb_2O_5/C.

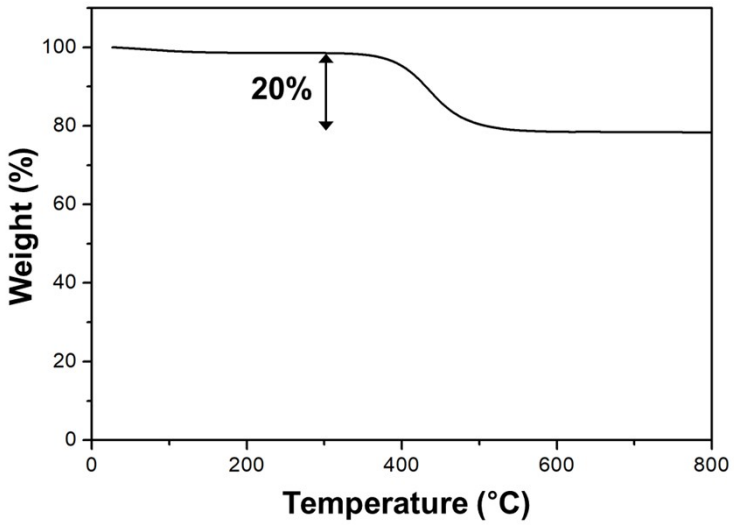

Fig. S6. TGA profile of m−Nb_2O_5/C.

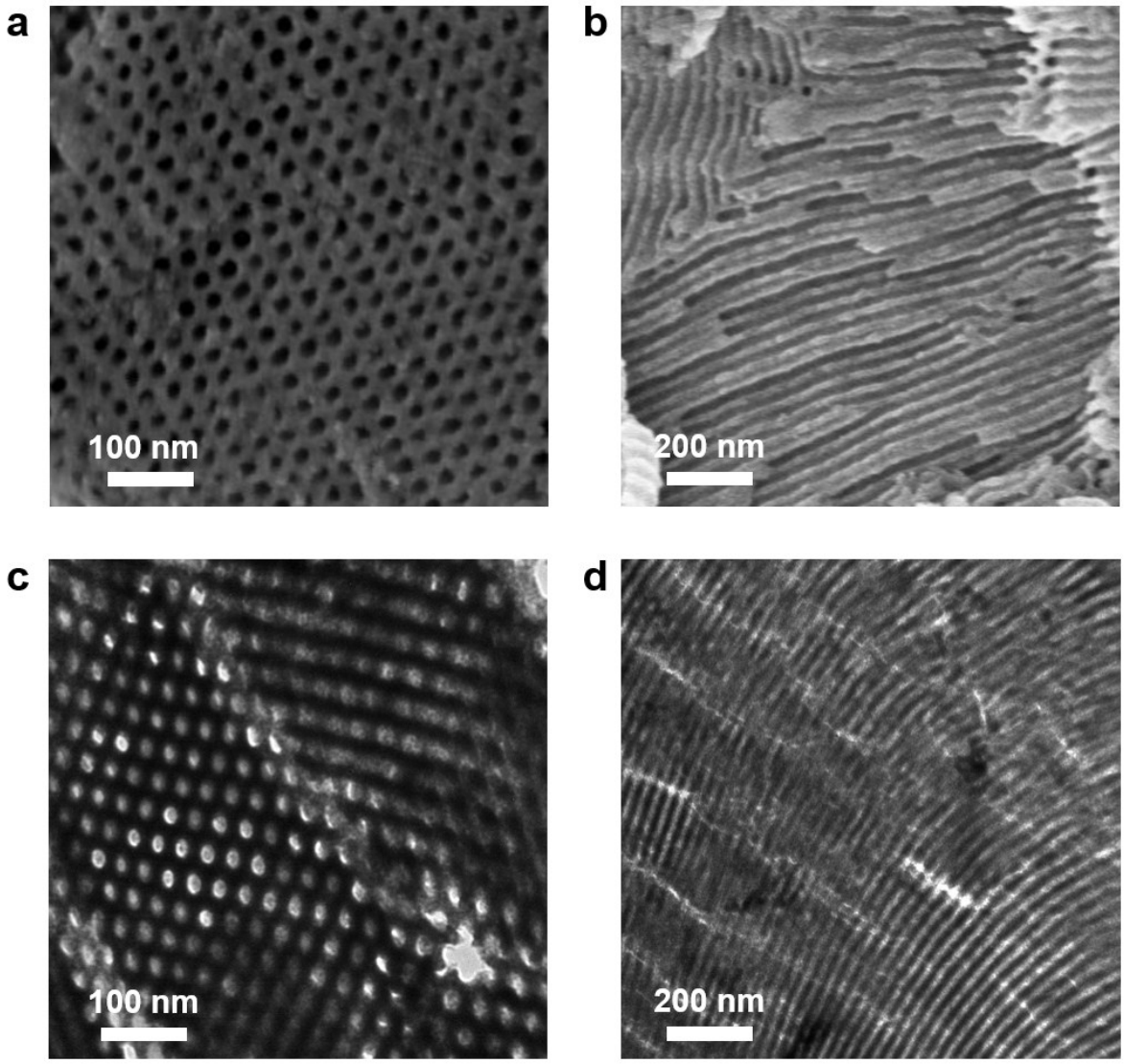

Fig. S7. (a, b) SEM and (c, d) TEM images of m−NbN/NC.

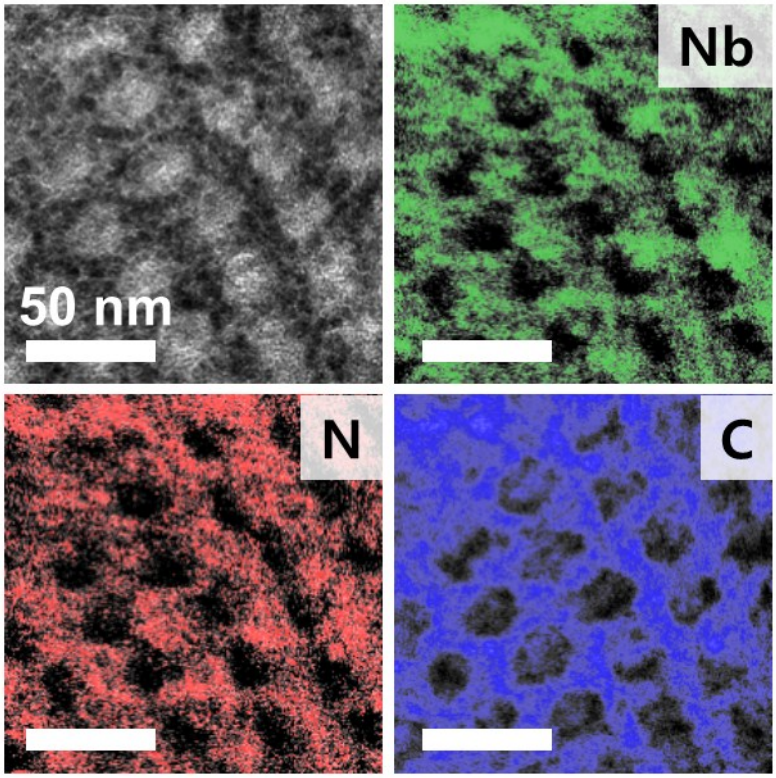

Fig. S8. EELS mapping results for niobium, nitrogen and carbon.

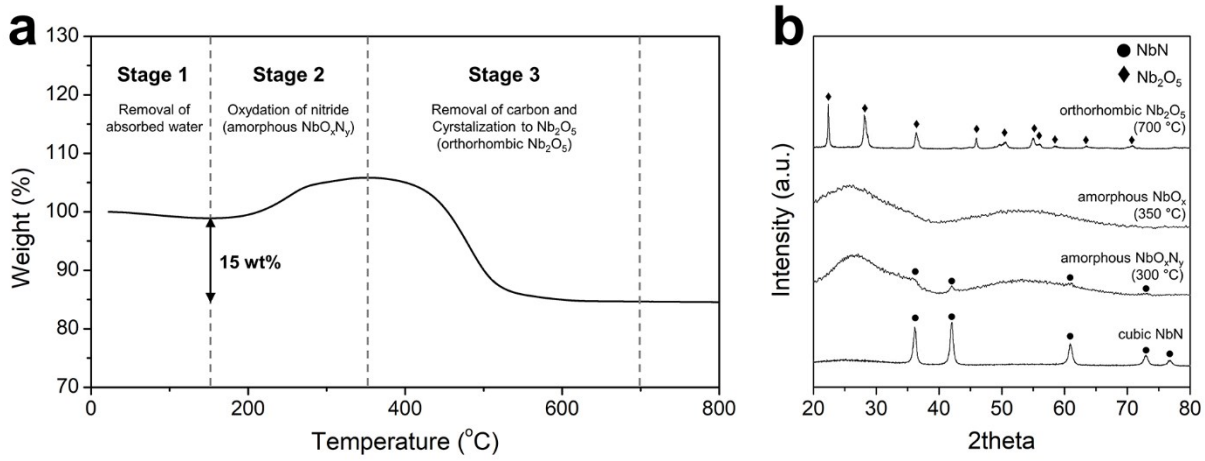

Fig. S9. (a) TGA profile of m-NbN/NC and (b) XRD patterns during the removal of carbon at 20 – 800 °C.

Carbon removal process of m-NbN/NC in the TGA profile can be divided into three stages: stage 1 for the removal of adsorbed water; stage 2 for the oxidation of NbN; stage 3 for the removal of carbon (Fig. S9a). In stage 2, the weight of NbN increased as cubic phase nitride was oxidized to amorphous Nb oxynitride (NbO_xN_y) at 150–350 °C. The cubic phase and amorphous phase were mixed at 300 °C. Entire nitride was converted into amorphous oxide species (NbO_x) which has higher molecular weight than NbN, and crystalline peaks were undetected at 350 °C (Fig. S9b). In stage 3, carbon was removed at 350–600 °C and amorphous NbO_x was crystallized into orthorhombic Nb_2O_5 phase at 700 °C. The carbon content of m-NbN/NC is estimated as approximately 15 wt% calculated by subtracting the final weight from the initial weight (Fig. S9a). The weight loss of carbon (5 wt%) was attributed to decomposition by hydrogen released from NH_3 during nitridation.

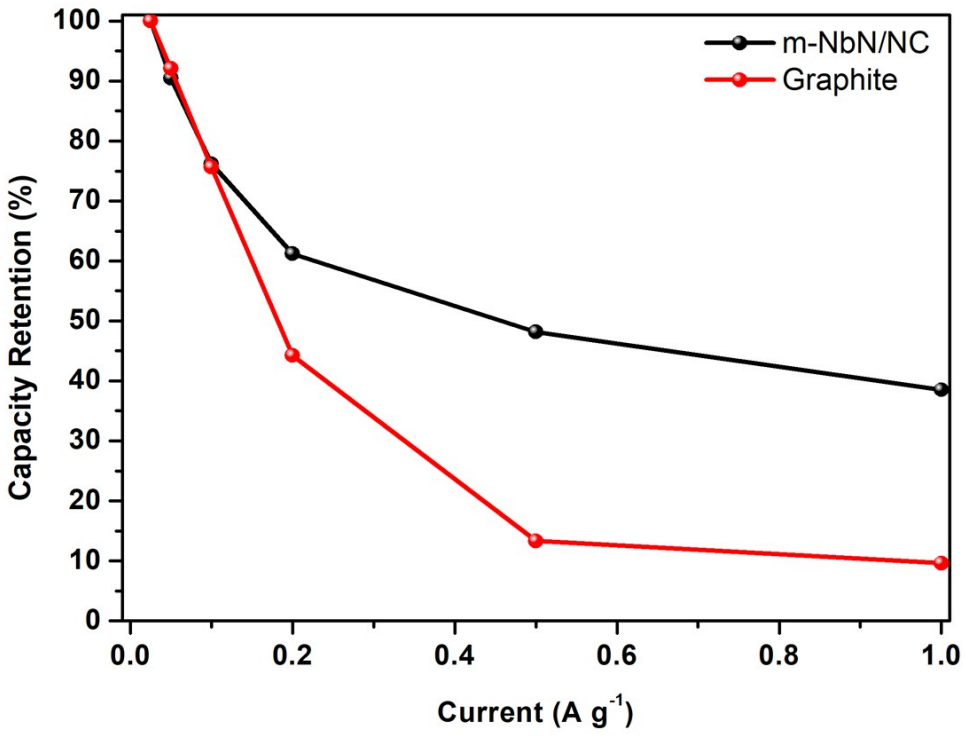

Fig. S10. The capacity retention of m−NbN/NC (black line) and commercial graphite (red line) at increasing currents.

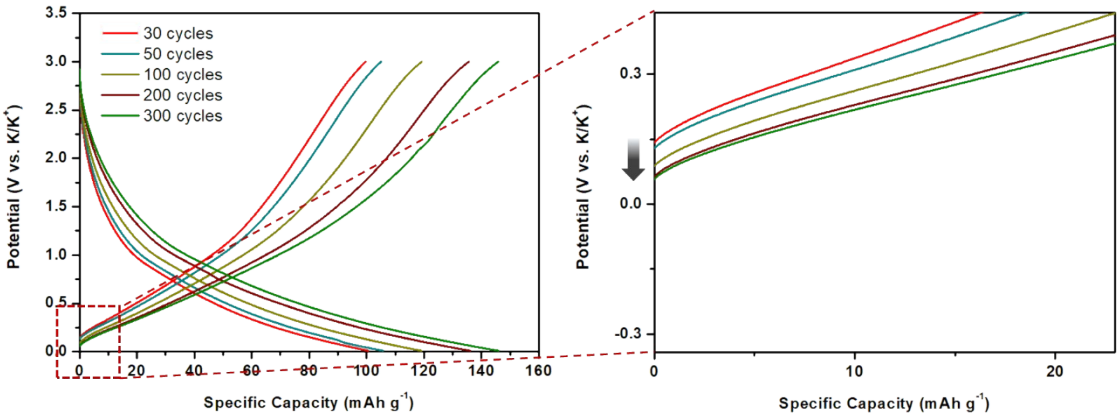

Fig. S11. Galvanostatic charge/discharge voltage profile at different cycles and enlarged specific area around 0.15 V vs. K/K^+ showing change of polarization.

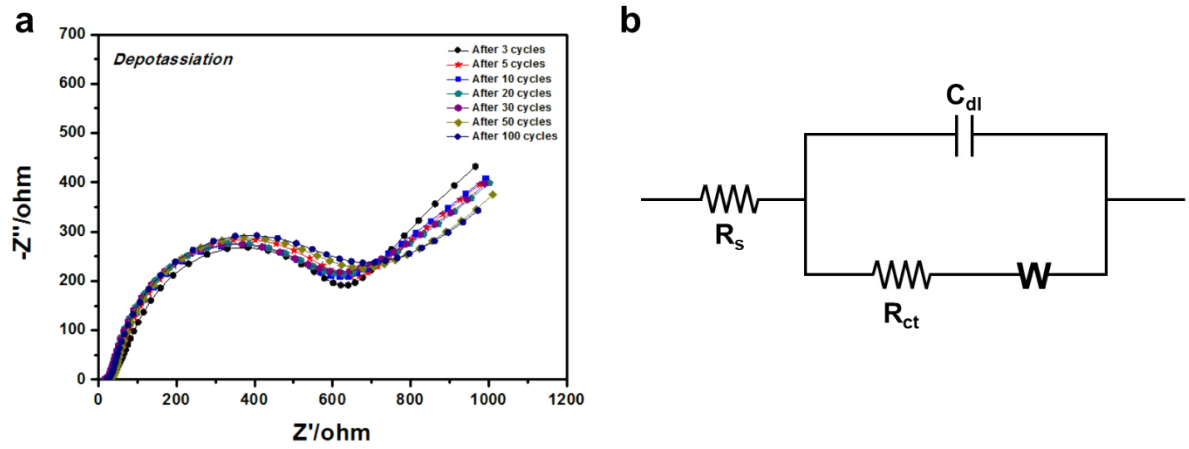

Fig. S12. (a) Nyquist plots of the m−NbN/NC at different cycles corresponding to (b) Equivalent circuit used to model the EIS data.

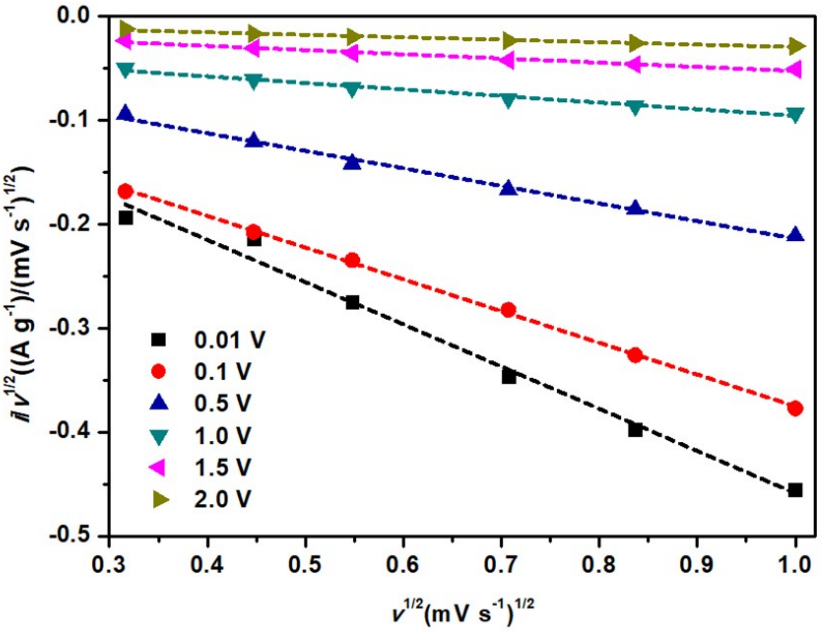

Fig. S13. Relationship between $i/v^{1/2}$ versus $v^{1/2}$ to calculate k_1 (slope) and k_2 (intercept) values at the various cathodic potential.

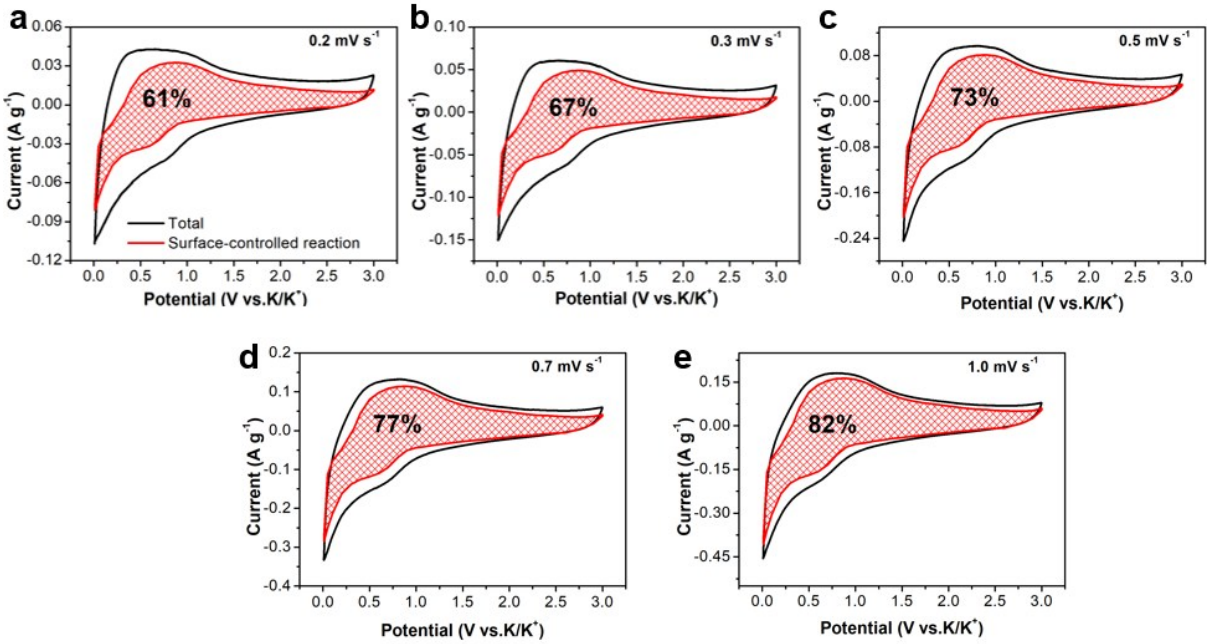

Fig. S14. The surface−controlled contribution of m−NbN/NC at various scan rates at (a) 0.2, (b) 0.3, (c) 0.5, (d) 0.7, and (e) 1.0 mV s^{-1}, respectively.

Table S1. The cyclic performance of previously reported carbonaceous anodes for KIBs.

Anode materials	Current density (mA g^{-1})	Cycle number	Capacity retention (%)	Ref.
m−NbN/NC	50	450	>100	This work
	500	2000		
Graphite	139	50	50	[1]
Soft carbon	558	50	81	[1]
N−doped Graphene	100	100	78	[2]
Hard Carbon Microsphere	28	100	83	[3]
Hard−Soft Composite Carbon	279	200	93	[4]
Amorphous Ordered mesoporous carbon	50	100	90	[5]
	1000	1000	74	
N, O co−doped hierarchically porous carbon	50	100	76	[6]
3D rGO aerogel	93	100	78	[7]

References

1. Z. Jian, W. Luo and X. Ji, *J. Am. Chem. Soc.*, 2015, **137**, 11566-11569.

2. K. Share, A. P. Cohn, R. Carter, B. Rogers and C. L. Pint, *ACS Nano*, 2016, **10**, 9738-9744.

3. Z. Jian, Z. Xing, C. Bommier, Z. Li and X. Ji, *Adv. Energy Mater.*, 2016, **6**, 1501874.

4. Z. Jian, S. Hwang, Z. Li, A. S. Hernandez, X. Wang, Z. Xing, D. Su and X. Ji, *Adv. Funct. Mater.*, 2017, **27**, 1700324.

5. W. Wang, J. Zhou, Z. Wang, L. Zhao, P. Li, Y. Yang, C. Yang, H. Huang and S. Guo, *Adv. Energy Mater.*, 2018, **8**, 1701648.

6. Y. Sun, H. Xiao, H. Li, Y. He, Y. Zhang, Y. Hu, Z. Ju, Q. Zhuang and Y. Cui, *Chem. Eur. J.*, 2019, **25**, 7359-7365.

7. L. Liu, Z. Lin, J.-Y. Chane-Ching, H. Shao, P.-L. Taberna and P. Simon, *Energy Storage Mater.*, 2019, **19**, 306-313.